

Analysis of the Reemergence of Winter Anomalies of Upper Ocean Characteristics in the North Atlantic from Reanalysis Data

P. A. Sukhonos^{a, *} and N. A. Diansky^{b, c, d, **}

^a *Institute of Natural and Technical Systems, Sevastopol, 299011 Russia*

^b *Moscow State University, Moscow, 119991 Russia*

^c *Marchuk Institute of Numerical Mathematics, Russian Academy of Sciences, Moscow, 119333 Russia*

^d *Zubov State Oceanographic Institute, Moscow, 119034 Russia*

**e-mail: pasukhonis@mail.ru*

***e-mail: nikolay.diansky@gmail.com*

Received August 26, 2020; revised October 27, 2020; accepted December 9, 2020

Abstract—On the basis of data from reanalysis and objective analysis for the second half of the 20th century, it is confirmed that the reemergence of anomalies of the characteristics of the upper mixed layer (UML) during the next year after their occurrence is possible in most of the North Atlantic (NA). Exceptions are regions near the western boundary currents and south of 15° N. The extracted signal is very pronounced in the leading empirical orthogonal functions (EOFs) of the UML temperature and mixed-layer depth, with contributions to the total variance of 17.9 and 23.9%, respectively, thus indicating the importance of this process in generating the anomalies of the upper ocean characteristics. The leading EOFs of the UML temperature and mixed-layer depth for 1959–2011, after the removal of third-order polynomials and the annual cycle, have a well-known tripole structure associated with the North Atlantic Oscillation. The EOF analysis in the time–depth plane for the Sargasso Sea and the northeastern NA demonstrates the process of reemergence of temperature anomalies at the ocean surface. The temperature anomalies formed throughout the UML in the period of its greatest winter deepening in February–March persist at depths of 50–200 m for the Sargasso Sea and 50–300 m for the northeastern NA throughout the year. These deep anomalies emerge at the surface in December, the period of the beginning of winter mixing. Subsurface temperature anomalies for 15 months (January–March of the next year) extend deep to the ocean, where they finally dissipate.

Keywords: reemergence of anomalies, upper mixed layer, North Atlantic

DOI: 10.1134/S0001433821030099

INTRODUCTION

It is hypothesized that at middle latitudes vigorous air–sea heat exchange during winter creates ocean temperature anomalies within a winter upper mixed layer (UML) [1, 2]. In the spring and summer warming period, the UML shoals and winter anomalies of the UML temperature are stored beneath a thin UML. These temperature anomalies may become reentrained into the UML when it deepens in the following fall and winter, thus influencing sea-surface temperature anomalies (SSTAs) in the following winter. Moreover, this behavior of SSTA should be closely tied to the seasonal evolution of the ocean UML depth. In this way, the SSTAs formed in winter would recur from one winter to the next without persistence at the surface through the summer.

The hypothesis was tested using observations from ocean weather stations C, D, E, and H in the North Atlantic (NA) and P and N in the Pacific Ocean and examined with a mixed-layer model [3].

The occurrence of SSTAs formed in the previous winter was termed the “reemergence mechanism.” The reemergence process may contribute considerably to generating SSTA in the NA on interannual to decadal scales [4]. These results highlight the important role the reemergence of SSTA plays in driving long-term changes in the SST field.

The SSTA can undergo the reemergence process in an individual region if the UML is much deeper in winter than in summer, currents in the upper ocean layer are relatively weak, and SSTAs of one sign occur over broad areas [5]. However, the SSTA reemergence was also detected in the vicinity of the Gulf Stream away from where SSTAs were formed in the previous winter [6]. Temperature anomalies could be advected away in the upper ocean layer, and water subduction weakens the reemergence of SSTA. The results [5, 6] show that the reemergence of SSTAs during the following year after their formation can be both collocated and remote. In the former case, SSTAs emerge where they formed in the previous winter. In the latter

case, the recurrence area is situated at a different location from a source region of the winter SSTAs as a result of water movement in the upper ocean layer.

The factors essential for the recurrence of SSTAs during the following year after their formation are substantially different at tropical and subtropical latitudes. In midlatitudes, the seasonal evolution of the UML depth plays a major role in this process [2, 3, 7]. The reemergence of SSTA at tropical locations may be linked to the recurrent anomalous atmospheric forcing, expressed by changes in the net surface heat flux and wind stress [8]. Teleconnections associated with ocean–atmosphere coupled climate modes, e.g., El Niño–Southern Oscillation (ENSO), may be one of the causes of this process [9]. A potential source for the recurrence of atmospheric forcing can be the seasonal variability of the storm-track positions, which is not affected by climate modes such as ENSO and the North Atlantic Oscillation (NAO) [7]. Note that the above forcing cannot be a manifestation of only atmospheric circulation eigenoscillations, a major energy of which is accounted for by synoptic [10] and low-frequency variability on time scales of 20–30 days [11, 12]. The issue of atmospheric memory is beyond the scope of the paper and needs a separate study.

Wintertime NA SSTAs reemerging in the following year after their formation may influence atmospheric circulation in the Atlantic–European region. The reemergence process may have a significant impact on the NAO [13, 14] and European weather conditions [15–17]. Note that summer–fall SSTAs in the NA may also influence winter characteristics of the atmospheric circulation, though not as strongly as in the fall and early winter [18].

In many studies, the analysis of SSTA reemergence is performed by calculating lag autocorrelation coefficients within the SSTA time series confined to particular coordinates or averaged within a certain ocean region in different instants of time. The autocorrelation function at some lag has a minimum and, with increasing lag, reaches a maximum that must be statistically significant. With this approach, for significant correlation coefficients at the 99% confidence level, seven recurrence areas in oceans around the world were detected [19]. All of these areas correspond to the regions where intermediate waters are formed in winter.

In [8], the recurrence of SSTA is detected by calculating the difference between 12- and 6-month lag autocorrelations. The 6-month lag corresponds to the summer months relative to the choice of a cold season from which the lag is counted. This difference is defined as the SSTA “reemergence index” [8]. The analysis of the difference between 12- and 6-month lag correlation coefficients has shown that the recurrence of SSTA is widespread in most of the global ocean. The exception is the equatorial central and eastern Pacific, where the variability driven by the ENSO process is dominant.

One method of objective analysis of the SSTA reemergence is an expansion of the upper ocean temperature anomalies in empirical orthogonal functions (EOFs) [4, 5]. The distinct feature of EOF analysis is its ability to detect coherent patterns of recurrent temperature anomalies by incorporating information in the original anomaly field from all grid points of the study area. It is this procedure that is used in our paper.

The goal of this paper is to examine features of the reemergence of winter anomalies of UML characteristics in the NA using ocean reanalyses and objective analyses spanning the second half of the 20th century.

DATA AND PROCESSING METHOD

The data used in the paper are monthly mean values of upper ocean temperature and UML depth from the Ocean Reanalysis System 3 (ORA-S3) [20], Geophysical Fluid Dynamics Laboratory (GFDL) reanalysis [21], Global Ocean Data Assimilation System (GODAS) [22], and Global Ocean Reanalysis and Simulation (GLORYS2V4) [23]. A description of the reanalysis datasets is given in Table 1. Monthly means of upper ocean temperature with one-degree spatial resolution taken from the objective analysis datasets of Ishii for 1945–2012 [24] and EN4.1.1 for 1945–2016 [25] (with a set of corrections by Gouretski [26]) were also used.

The datasets have a different spatial resolution in the horizontal and vertical. All calculations are performed at the initial spatial resolution of the data. Prior to computations, third-order polynomials were subtracted from the time series of the ORA-S3 and GFDL reanalyses and Ishii and EN4.1.1 objective analyses at each grid point to remove the low-frequency variability. From the GODAS and GLORYS2V4 time series, only first-order polynomials (linear trends) were subtracted because of their short duration (in a climatic sense). The polynomial coefficients were calculated by the least-squares method. Next the annual cycle (long-term averages for each month of the year for the available period) was removed at each grid point in all the datasets. The resulting anomalies were then expanded in EOFs. The correlation and spectral analysis methods were used in the paper. Time spectra were calculated from the ORA-S3 and GFDL reanalyses and Ishii and EN4.1.1 objective analyses for the available period using a spectral Tukey window [27]. The length of the correlation function was 20 years to provide seven to nine degrees of freedom. Confidence intervals were calculated using a χ^2 distribution.

RESULTS

The authors’ comparative examination of the long-term ocean reanalyses has shown that the ORA-S3 can be considered most representative of the goal to be sought [28]. For this reason, the present paper consid-

Table 1. Description of the reanalyses

Reanalysis	Ocean model, configuration	Atmospheric forcing	Assimilation procedure, data	Period	UML depth criterion
ORA-S3 [20]	HOPE, $1^\circ \times 1^\circ$, $\sim 1^\circ \times 0.3^\circ$ at the equator; 29 levels	ERA-40 before June 2002, then opera- tional analysis	MvOI. T, S, SSH	1959–2011	$Ri_{crit} = 0.3$
GFDL [21]	MOM4 coupled, $1^\circ \times 1^\circ$, $\sim 1^\circ \times 0.3^\circ$ at the equator; 50 levels	Coupled data assimilation	KF. T, S	1961–2015	$\Delta\rho = 0.03 \text{ kg/m}^3$
GODAS [22]	MOM3, $1^\circ \times 1^\circ$, $\sim 1^\circ \times 0.3^\circ$ at the equator; 40 levels	NCEP R2	3D-Var. T, S	1980–2018	$\Delta T = 0.8^\circ\text{C}$
GLORYS2V4 [23]	NEMO3.1, $0.25^\circ \times 0.25^\circ$; 75 levels	ERA-Interim	KF. T, S, SSH	1993–2015	$\Delta T = 0.2^\circ\text{C}$

T , S , and SSH are the observed temperature, salinity, and sea surface heights (satellite altimetry), respectively; MvOI is the multivariate optimal interpolation; 3D-Var is a three-dimensional variational analysis; KF is the Kalman filter; Ri_{crit} is the critical Richardson number; and $\Delta\rho$ (ΔT) is the increase in density (decrease in temperature) relative to their values at 10 m.

ers results obtained mainly from data of this reanalysis. The average long-term fields of the temperature and currents in the UML from the data reflect the climatological circulation in the NA quite well. The fields of these characteristics in Fig. 1 are given from the ORA-S3 reanalysis data. Regions with high current speeds and abrupt temperature changes in the UML are confined to the Gulf Stream and North Atlantic Current fronts. The estimates of the UML depth from the ORA-S3 data obtained using a Richardson number criterion give the best fit to the depth of convective mixing in the Labrador Sea during winter derived from field data [29]. The amplitude of the seasonal cycle of UML depth (February minus September) from ORA-S3 for 1959–2011 is spatially nonuniform (Fig. 1b). The UML depth south of 8° N is deeper in September than in February. The magnitudes of the amplitude in this region average 12 m. To the north of 20° N (30° N), the UML depth is 50 m (90 m) deeper in February than in September. To the north and west of the North Atlantic Current, in a region covering the Labrador Current and the interior of the subpolar gyre, the difference between UML depths in February and September exceeds 500 m. The largest amplitude of the seasonal cycle of UML depth occurs in the Labrador Sea, where its magnitudes exceed 2500 m. This is due to winter cooling and convective mixing in the UML. Thus, favorable conditions for the reemergence of anomalies of the UML characteristics, such as a developed winter convection, relatively weak currents, and no sharp temperature gradients [5], are common to most of the NA.

Next we consider lag correlations between time coefficients of the leading EOFs of the UML temperature and depth from the ORA-S3 monthly mean data

for all months for the period 1959–2011. The UML temperature is defined as the average temperature in the range from the surface to the UML base, whose position is variable in space and time. The EOF expansion is carried out using monthly mean anomaly fields in deviations from the average annual cycle and third-order polynomial trend for the period 1959–2011 in the NA region bounded by 15° – 70° N, 8° – 80° W. The following procedure of data processing proposed in [5] was used to remove the intraannual variability. Standard deviations (SD) averaged over the NA region are calculated for each calendar month of the whole period of 1959–2011 for UML temperature and depth anomalies. Their values lie in a range from 0.46°C in February to 0.65°C in August for the UML temperature and from 26 m in August to 90 m in April for the UML depth. Then the anomalies of the UML temperature and depth at each grid point for each month are scaled by normalizing by their basin-averaged SD. The EOFs were then computed for the dimensionless UML temperature and depth anomaly fields taking into account the cosine of latitude. The region south of 15° N was not used in the EOF expansion of the UML temperature and depth fields to remove the equatorial variability modes, where the half-year harmonic makes a major contribution to the annual cycle. Moreover, the difference in the UML depth between February and September is small here (see Fig. 1b).

The spatial patterns of the leading EOFs of the UML temperature and depth in the NA represent a well-known tripole structure (Fig. 2). Changes in UML temperature and depth are of one sign at tropical and subpolar latitudes and the opposite sign at subtropical latitudes. A northern cell of the tripole pattern corresponding to deep convection in the interior of the

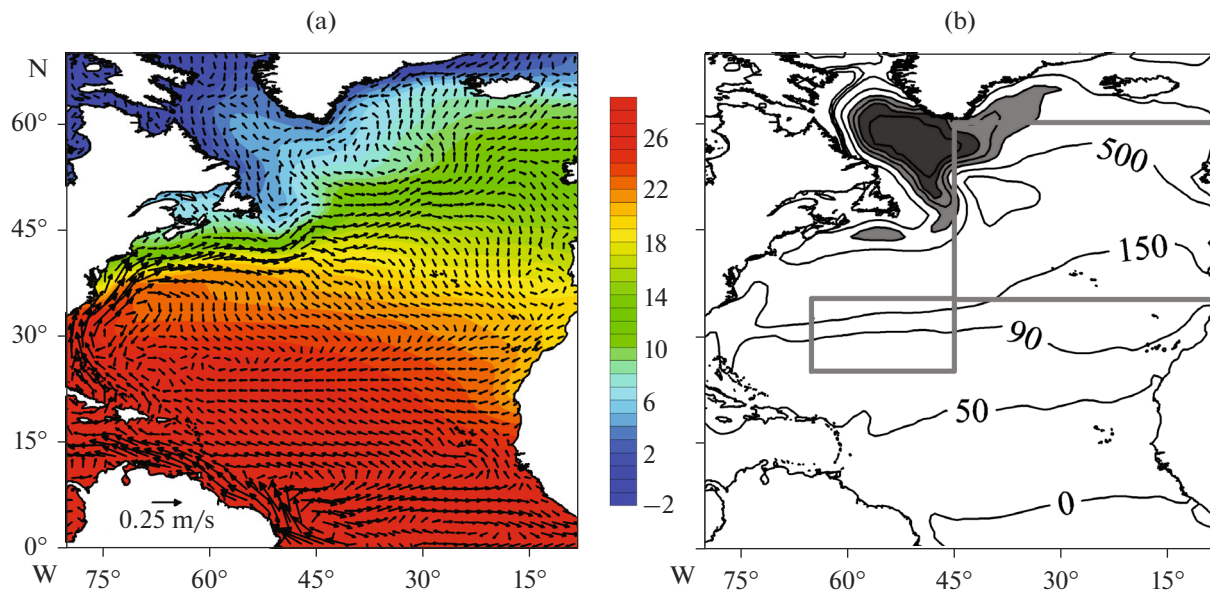


Fig. 1. (a) Average current speed in the UML (vectors, m/s) and average UML temperature (shading at 1°C) in the North Atlantic for 1959–2011. (b) Amplitude of the seasonal cycle of UML depth (February minus September) for the given period; isolines are plotted at 0, 50, 90, 150, 500, 1000, 1500, 2000, and 2500. Regions in which the amplitude exceeds 1000 m (2000 m) are shown in light gray (dark gray). Two study regions are shown by gray rectangles: the Sargasso Sea (25° – 35° N, 65° – 45° W) and the northeastern NA (35° – 60° N, 45° – 8° W). The fields in the figure are from the ORA-S3 reanalysis data.

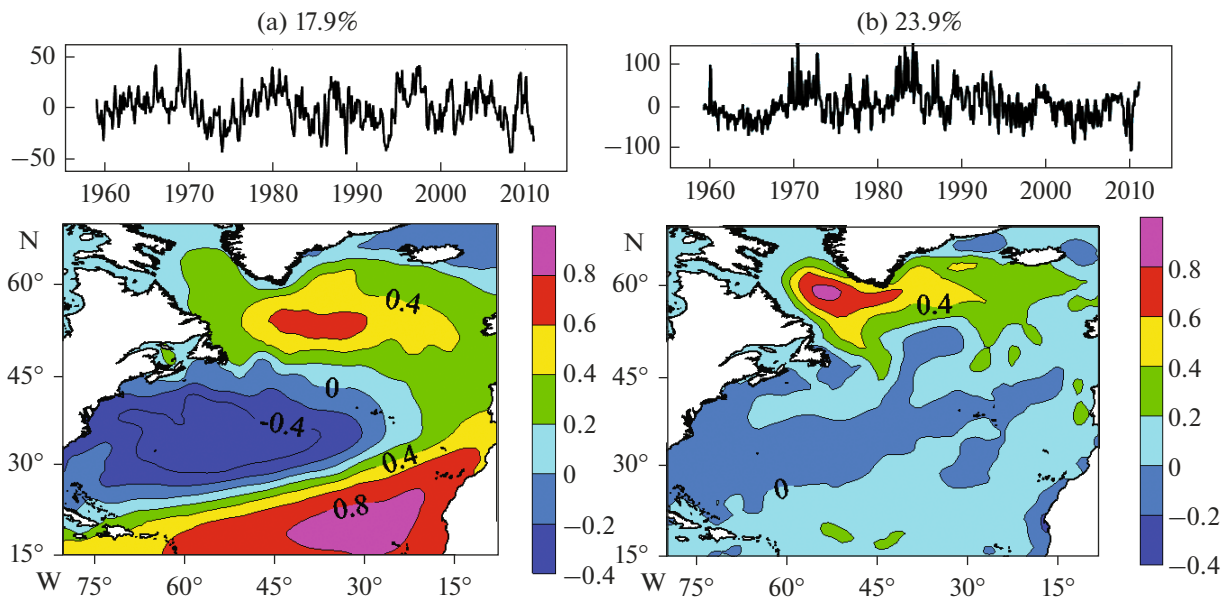


Fig. 2. Time coefficients and leading EOFs of the monthly means of (a) UML temperature and (b) depth for 1959–2011. Third-order polynomials and the annual cycle are removed; data in each month are normalized by their space-averaged SD. The spatial EOF pattern is shown as the correlation between the time coefficient and UML temperature and depth anomalies for the period available. Isolines are plotted at 0.2. The value at the top of the panel is the fraction of the variance explained by this EOF.

subpolar gyre is most pronounced in the spatial structure of the leading EOF of the UML depth.

Correlations of the time coefficient of leading EOFs (Fig. 2), from a sample for each calendar month (vertical axis), with time coefficients in the subsequent

months at lags from 0 to +12 months (horizontal axis) are shown in Fig. 3 for the UML temperature and depth, respectively. Correlations of the time coefficients of the leading EOF of UML temperature for all calendar months decay at a lag of 3–4 months (Fig. 3a).

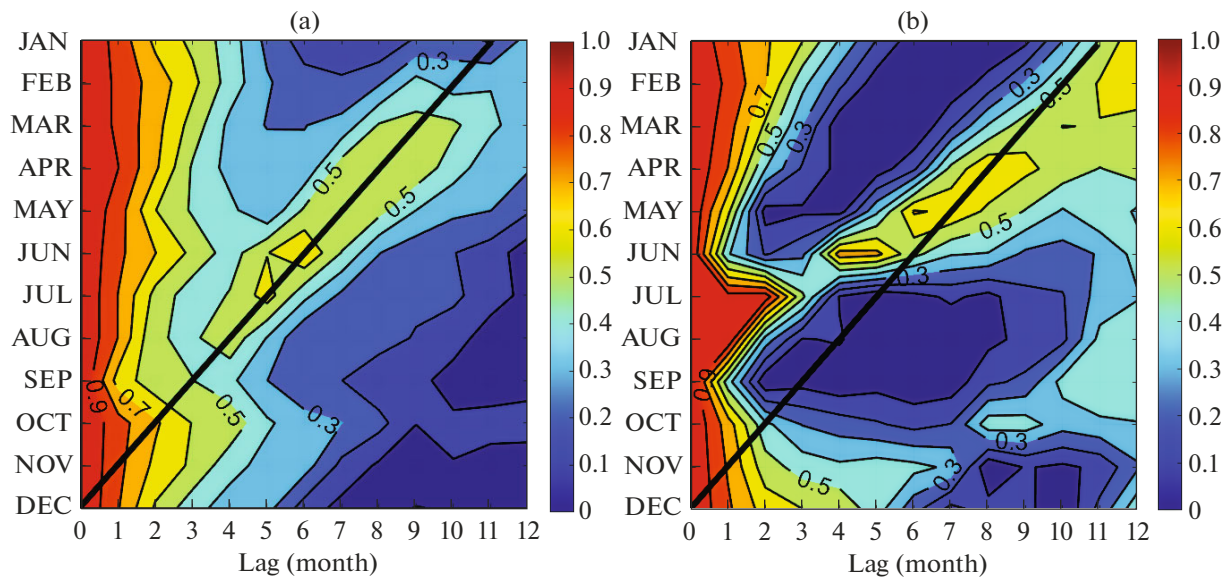


Fig. 3. Lag correlations between time coefficients of the leading EOF of (a) UML temperature and (b) depth from Fig. 2 calculated separately for each calendar month from ORA-S3 for the period 1959–2011. Contour interval is 0.1. The black diagonal line is a visual aid in locating December.

However, the correlation coefficients for months from February through July first drop and then rise as the lag increases from a half-year to 11 months. The largest correlation coefficients are obtained for June and July at a lag of 5–6 months. The correlation coefficients for the fall months do not decrease in the following year. The most rapid decline occurs in September. Such a correlation structure for the time coefficient of the leading EOF of UML temperature confirms the possibility for the reemergence of the UML temperature anomalies formed in the late winter and early spring.

Correlations of the time coefficient of the leading EOF of the UML depth for spring and fall months at lags of 1–4 months decrease faster than their counterparts with a lag from winter and summer months (Fig. 3b). The correlation coefficients with a lag from winter, spring, and summer months first drop and then rise with increasing lag. The correlations for the time coefficient of the leading EOF in February increase from less than 0.45 at a 3-month lag (May) to greater than 0.6 when the lag is 11 months (January). The anomalies of UML depth in June recover 4 or 5 months later, when vigorous convection develops in the following fall and winter. For the UML depth anomalies formed in late summer, the correlation coefficients do not show any increase at large lags, which also confirms the hypothesis of reemergence of anomalies of the UML characteristics. The time coefficient of the second EOF for each calendar month for both UML temperature anomalies and UML depth anomalies (not shown) also contains the reemergence signal, although it is weaker than in the leading EOF. Thus, the UML depth anomalies can persist from one

winter to the next with the recurrent UML temperature anomalies.

The formation of the recurrent anomalies of UML temperature and depth is not uniform throughout the NA. According to the results of [5, 19], two regions with intense manifestations of recurrent SSTAs were detected in the NA: in the Sargasso Sea (25° – 35° N, 65° – 45° W) and in the northeastern NA (35° – 60° N, 45° – 8° W). Their borders are shown in Fig. 1b. These regions correspond to the subtropical and subpolar cells with opposite signs on the tripole pattern of the leading EOF. Coherent patterns of the recurrent anomalies in these regions will be analyzed using the procedure from [5], but incorporating new and longer term reanalysis and objective analysis data. Temperature anomalies were averaged over the regions so as to form a field in the time–depth plane. The EOF for the Sargasso Sea was calculated as follows. The temperature value on a spatial grid from specified horizons in the 0–300 m layer and 15 months (January to the next March) is the observational vector for each year of the available period. In the 0–300 m layer, data are given at 19 levels in ORA-S3, at 27 levels in GFDL, at 26 levels in GODAS, and at 35 levels in GLORYS2V4. Within 0–300 m, the data in the Ishii objective analysis are given at 12 levels and data in EN4.1.1 are at 20 levels. The EOF calculation for the northeast NA was carried out similarly, except for the choice of the 0–550 m layer.

Correlation coefficients between temperature anomalies within a 15-month interval (January to March of the following year) detected by EOF analysis are shown for the Sargasso Sea in Fig. 4. The leading EOF in the time–depth plane explains nearly 50% of the

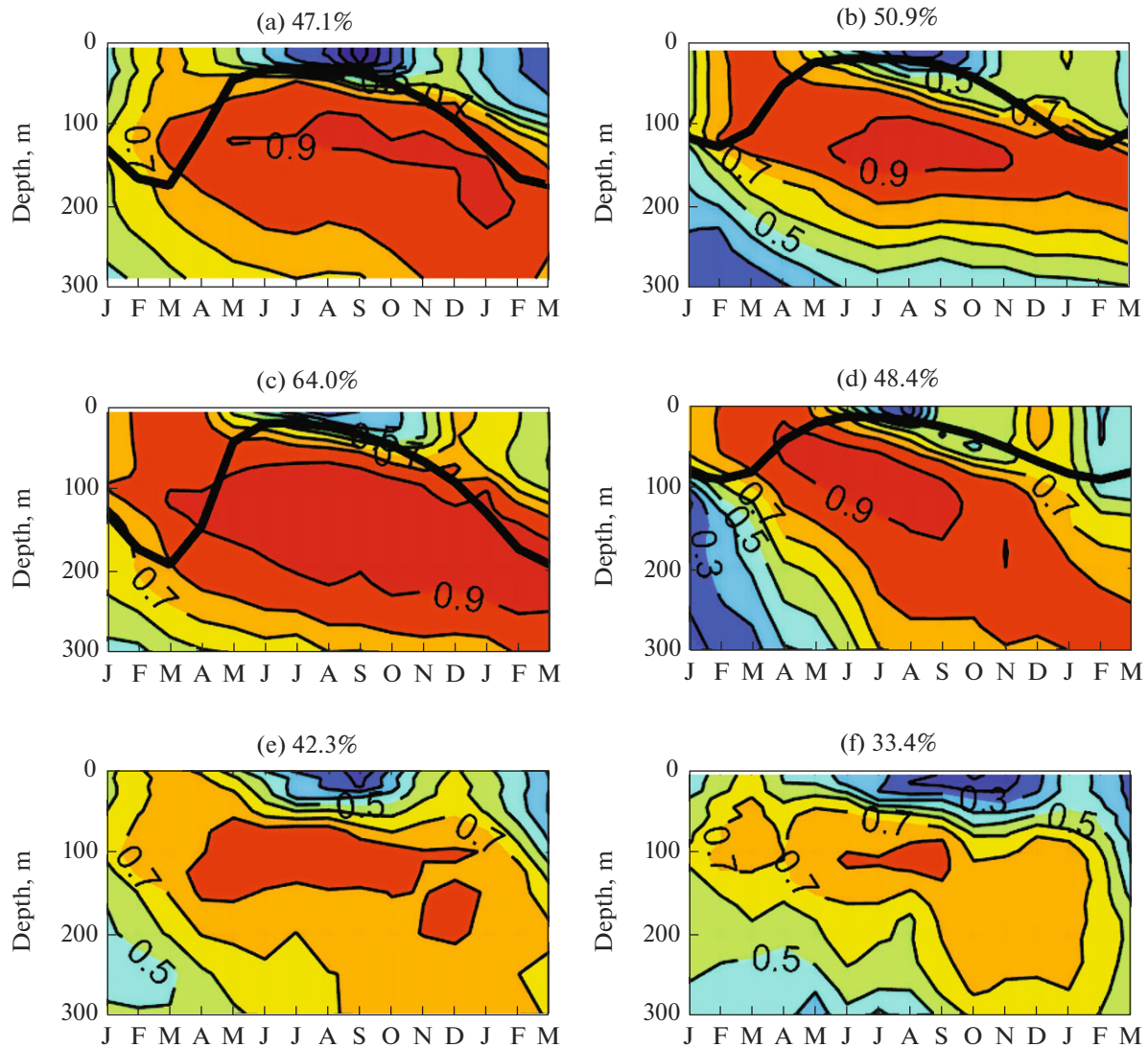


Fig. 4. Time–depth pattern of the leading EOF for 25° – 35° N, 65° – 45° W from (a) ORA-S3, (b) GFDL, (c) GODAS, and (d) GLORYS2v4 reanalyses and (e) Ishii and (f) EN4.1.1 objective analyses. The value at the top of each panel is the fraction of the variance explained by this EOF. EOF calculation was performed from January to March of the following year and from the surface to a depth of 300 m. The EOF pattern is shown as the correlation between time coefficient and temperature anomalies for the available period. Contour interval is 0.1. The thick black line in (a)–(d) is the average UML depth in the region.

variance. The correlation coefficients at the surface (0–30 m) decrease from May to November, while at large depths (70–150 m) they barely decay in these months. All the EOFs demonstrate the formation of temperature anomalies within the UML in the period of its maximum winter deepening in March and their persistence at a depth of 50–200 m throughout year, with their gradual deepening by the end of the 15 months. These deep anomalies appear at the surface in December, the month of the beginning of winter mixing, as a result of which the anomalies are reentrained into the surface layer. This signal shows up in magnitudes of the correlation coefficients greater than 0.5 until the following March, when the newly developed spring–summer UML comes into play. The reemergence of

SSTA is most distinct in the GODAS data (the first EOF explains the largest fraction of the variance, 64%) and less visible in the EN4.1.1 data (the first EOF explains the least variance, 33.4%). The average UML depth over the available period in the given region in late winter and early spring is 175 m from the ORA-S3 data, 124 m from GFDL, 193 m from GODAS, and 91 m from GLORYS2V4. Subsurface temperature anomalies for 15 months extend deep into the ocean, where they finally dissipate.

The structure of the regional EOF for the north-eastern NA obtained from the datasets used is shown in Fig. 5. Temperature anomalies in the UML that are formed when it maximally deepens during winter in February–March are stored at 50–300 m through the

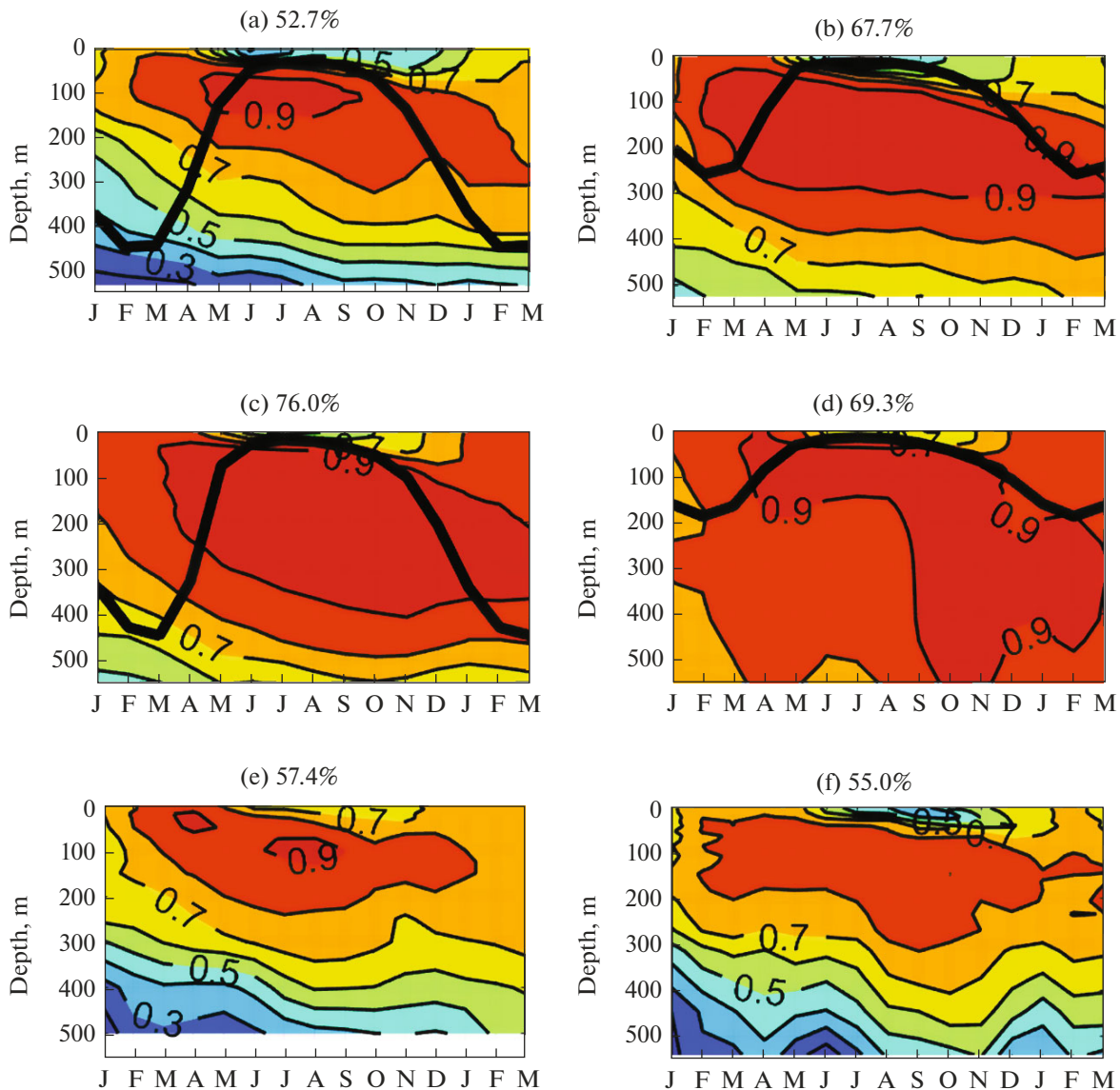


Fig. 5. Time–depth pattern of the leading EOF for 35° – 60° N, 45° – 8° W from (a) ORA-S3, (b) GFDL, (c) GODAS, and (d) GLORYS2v4 reanalyses and (e) the Ishii and (f) EN4.1.1 objective analyses. The value at the top of each panel is the fraction of the variance explained by this EOF. EOF calculation was performed from January to March of the following year and from the surface to a depth of 550 m. The EOF pattern is shown as the correlation between time coefficients and temperature anomalies for the available period. Contour interval is 0.1. The thick black line in (a–d) indicates the average UML depth.

spring and summer. The first EOF for this region explains the largest variance (76%) from the GODAS data and the least variance (52.7%) from the ORA-S3. The average UML depth over the available period in the northeastern NA in late winter and early spring is 445 m from the ORA-S3 data, 260 m from GFDL, 447 m from GODAS, and 188 m from GLORYS2V4. Thus, the UML temperature anomalies formed in summer are stored in the UML. The winter UML temperature anomalies remain beneath the UML in summer and become reentrained into the UML when it deepens in the following fall and early winter. This is broadly consistent with the concept of the SSTA reemergence.

The time coefficients of the regional temperature EOFs for the Sargasso Sea and the northeastern NA are shown in Fig. 6. The correlation without lag between time coefficients of temperature EOFs for these regions is negative. Synchronous correlation coefficients for the time series from the ORA-S3 and GFDL data are -0.46 and -0.45 , respectively. The time coefficients of temperature EOFs from all the datasets for the Sargasso Sea have absolute minima in 1970 and 2010 (Fig. 6a). Spectral analysis of the time series in Fig. 6 shows significant periodicities of the reemergence signal around 4.5 and 12–14 years. The analysis of the cross-correlation functions between time series in Figs. 6a and 6b revealed a significant

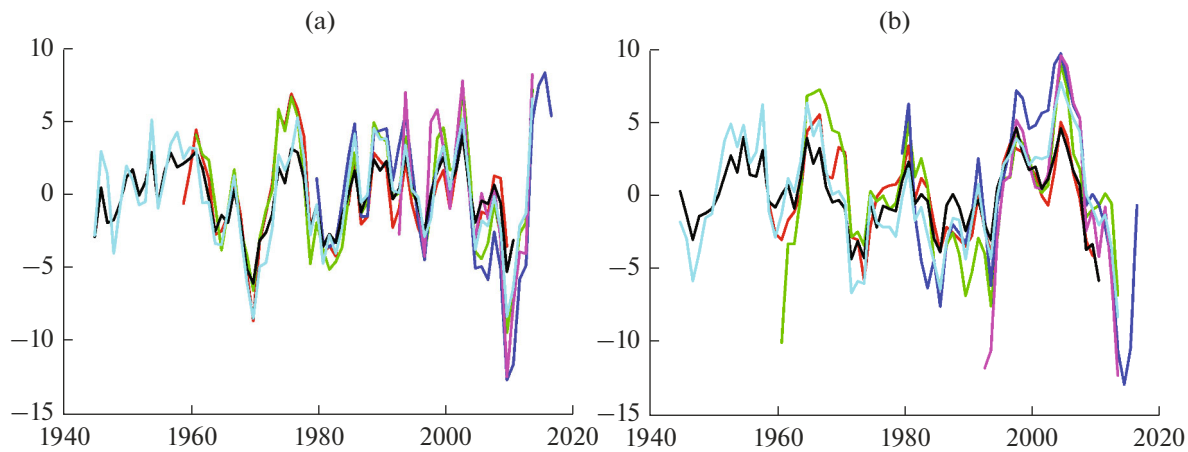


Fig. 6. EOF time coefficients for (a) 25° – 35° N, 65° – 45° W and (b) 35° – 60° N, 45° – 8° W. EOF calculation was performed from January to March of the following year and from the surface to (a) 300 and (b) 550 m. Data from ORA-S3 (red), GFDL (green), GODAS (blue), GLORYS2V4 (magenta), Ishii (black), and EN4.1.1 (cyan).

connection at the 95% confidence level for the 4-year leading of the time coefficients of EOF for the Sargasso Sea. The correlation coefficients at this lag are 0.41 for time series from ORA-S3, 0.36 for GFDL, 0.50 for GODAS, 0.50 for Ishii, and 0.44 for EN4.1.1.

DISCUSSION OF RESULTS

The results from numerous studies in the NA have revealed a stable mode of the interannual SST variability that has a tripole structure. The tripole-type variability is coupled to the variability of the NAO and is also typical of the UML depth and net surface heat fluxes (see, e.g., [30]). A model study of the relative role of surface heat fluxes and upper ocean processes in generating the tripole structure has shown that upper ocean processes estimated as a residual of the heat balance equation play an important role in the heat budget of the NA waters [31]. An examination of the relative role of all the terms of the UML heat balance equation in the tripole variability from the ORA-S3 data for 1959–2011 has shown that the budget of the different terms of the integral heat balance equation for the UML determines the evolution of the UML characteristics in various parts of the NA [32].

The results from the EOF analysis of UML temperature and depth confirm that the reemergence of SSTA is likely to occur in most of the NA. Moreover, this signal is detected in the first and second EOF after the removal of polynomial trends and the annual cycle from the original data, which indicates the importance of this process in generating the anomalous upper-ocean structure, consistent with the results in [8]. At the same time, we have revealed that not only can SSTAs undergo reemergence, but UML depth anomalies are subject to reemergence. This confirms the possibility of preserving the anomalies of UML characteristics.

According to our results, the region of the small correlation coefficients on the EOF pattern in the time–depth plane in October also becomes deeper (Fig. 4), but less than estimated in [5]. Because around the Sargasso Sea the circulation is anticyclonic and the average UML depth in February–March from the ORA-S3 and GODAS data is over 170 m, depths deeper than 160 m (below the base of the UML) are required for the analysis of the reemergence signal. The reason is that the reemergence signal of the UML anomalies is very strong and extends to large depths. Taking large depths into account may increase the variance in the time–depth plane over 25° – 35° N, 65° – 45° W explained by the leading EOF.

Time coefficients of the leading EOF in the overlapping period (1955–1995) in Fig. 6a (this paper) and in Fig. 3a [5] are very consistent. Nonetheless, the values of the time coefficient derived from the datasets considered here are slightly overestimated. Overall, this implies that the datasets agree well with those of the paper cited above.

That the time coefficients of regional EOFs in Fig. 6 are out of phase is explained by the fact that the Sargasso Sea and the northeastern NA are situated in oppositely signed regions of the tripole pattern in the NA (see Fig. 2). Hence the synchronous anomalies of UML temperature also have opposite signs.

The time coefficients of the regional EOFs characterizing the SSTA reemergence signal for the Sargasso Sea have absolute minima in 1970 and 2010. Despite a sample error in the initial data, the period 1970–1974 shows some weakening of the Gulf Stream and of its recirculation compared to 1955–1959 [33]. A 30% slowdown in the thermohaline circulation in the NA for 14 months during 2009–2010 reduced northward meridional heat transport (MHT) across 25° N [34]. The recirculation of the Gulf Stream was suggested as a factor influencing the MHT at 26.5° N [35]. Accord-

ing to a model study [36], the anomalously low MHT in 2010 was due to a weaker anticyclonic recirculation in the western part of the subtropical gyre. Both periods, the late 1960s to the early 1970s and 2009–2010, exhibit significant weakening in NAO, which has changed Ekman transport and weakened the Gulf Stream [37].

The time coefficients of the regional temperature EOFs for the Sargasso Sea and the northeastern NA, describing the strength of the SSTA reemergence signal, have periodicities at scales of 4.5 and 12–14 years. Interannual oscillations with nearly 4-year periods are distinguished in the variability of advective heat transport in the UML in the Gulf Stream–North Atlantic Current system as well [38]. The singular spectral analysis of the NA SST field for 1901–1994 revealed a significant 13-year periodicity with an amplitude of about 0.5°C [39]. The spectral analysis of the SSTAs propagating along the Gulf Stream and the North Atlantic Current in the northeast direction revealed a peak at 12–14 years [40]. They propagated with an average velocity of 1.7 cm/s, and their amplitude was in the range 0.5–1.0°C. A significant 14-year spectral peak was detected in the subpolar North Atlantic and Nordic Seas [41]. It was attributed to the propagation of SSTA along the path of the North Atlantic and Norwegian currents with an average velocity of 2 cm/s. Thus, significant periodicities detected in the time coefficients of regional EOFs (Fig. 6) are due to the internal ocean variability.

CONCLUSIONS

An examination of the reemergence of winter anomalies of the UML characteristics in the NA using ocean reanalyses and objective analyses for the second half of the 20th century has shown the following results.

The reemergence of anomalies of the UML characteristics in the following year after their formation is likely to occur in most of the NA (north of 15° N). With no vigorous currents or sharp temperature gradients, the UML depth anomalies can persist from one winter to the next together with the recurrence of the UML temperature anomalies. This signal is recorded in the first and second EOFs, which confirms the importance of this process in shaping the anomalous structure of the upper ocean layer.

The leading EOFs of the UML temperature and depth after the removal of polynomial trends and the annual cycle have a tripole structure. The analysis of regional EOFs of the UML temperature for regions corresponding to the subtropical and subpolar areas of the tripole pattern has shown that UML temperature anomalies formed in summer persist in the UML. Winter temperature anomalies are stored beneath the UML through the summer and are reentrained into the UML when it deepens in the following fall and early winter. This is completely consistent with the

concept of SSTA reemergence. The contribution of the regional EOFs to the total variance of the upper ocean temperature is nearly 50%.

The EOF analysis in the time–depth plane for the selected NA regions demonstrates the SSTA reemergence process. Temperature anomalies begin to form within the entire UML in the period of its largest winter deepening in February–March. They remain at depths of 50–200 m throughout the year, gradually deepening by the following March. These deep anomalies appear at the surface in December (the period of the beginning of winter mixing), as a result of which they lift up to the surface. Subsurface temperature anomalies for 15 months extend deep to the ocean, where they finally dissipate.

The time coefficients of the regional temperature EOFs for the Sargasso Sea and the northeastern NA are synchronously out of phase. This is because these regions are located in the oppositely signed areas of the tripole pattern of the interannual variability of the NA UML temperature. For the 4-year leading of the time coefficients of EOF for the Sargasso Sea region, a significant positive correlation is found with time coefficients of EOF for the northeastern NA. The time coefficients of EOF for the Sargasso Sea region have absolute minima in 1970 and 2010. Time coefficients of regional temperature EOFs exhibit significant periodicities of the reemergence signal at 4.5 and 12–14 years. These periodicities are due to the internal ocean variability.

ACKNOWLEDGMENTS

We thank an anonymous reviewer for friendly and constructive criticism of the first version of the paper and the editorial board for their professional and prompt review of it.

FUNDING

The data were obtained and processed under State Task no. AAAA-A19-119040490047-7); the analysis of the regional anomaly reemergence was supported by the Russian Science Foundation, project no. 17-17-01295).

REFERENCES

1. J. Namias and R. M. Born, “Temporal coherence in North Pacific sea-surface temperature patterns,” *J. Geophys. Res.* **75**, 5952–5955 (1970).
2. J. Namias and R. M. Born, “Further studies of temporal coherence in North Pacific sea surface temperatures,” *J. Geophys. Res.* **79**, 797–798 (1974).
3. M. A. Alexander and C. Deser, “A mechanism for the recurrence of wintertime midlatitude SST anomalies,” *J. Phys. Oceanogr.* **25** (1), 122–137 (1995).
4. M. Watanabe and M. Kimoto, “On the persistence of decadal SST anomalies in the North Atlantic,” *J. Clim.* **13** (16), 3017–3028 (2000).

5. M. S. Timlin, M. A. Alexander, and C. Deser, "On the reemergence of North Atlantic SST anomalies," *J. Clim.* **15** (18), 2707–2712 (2002).
6. G. de Coetlogon and C. Frankignoul, "The persistence of winter sea surface temperature in the North Atlantic," *J. Clim.* **16** (9), 1364–1377 (2003).
<https://doi.org/10.1175/1520-0442-16.9.1364>
7. X. Zhao and J. Li, "Winter-to-winter recurrence of sea surface temperature anomalies in the Northern Hemisphere," *J. Clim.* **23** (14), 3835–3854 (2010).
<https://doi.org/10.1175/2009JCLI2583.1>
8. P. Byju, D. Dommengot, and M. A. Alexander, "Wide-spread reemergence of sea surface temperature anomalies in the global oceans, including tropical regions forced by reemerging winds," *Geophys. Res. Lett.* **45** (15), 7683–7691 (2018).
<https://doi.org/10.1029/2018GL079137>
9. J. Bjerknes, "Atmospheric teleconnections from the equatorial Pacific," *Mon. Weather Rev.* **97** (3), 163–172 (1969).
[https://doi.org/10.1175/1520-0493\(1969\)097<0163:ATFTEP>2.3.CO;2](https://doi.org/10.1175/1520-0493(1969)097<0163:ATFTEP>2.3.CO;2)
10. G. S. Golitsyn, *Introduction to Dynamics of Planetary Atmospheres* (Gidrometeoizdat, Leningrad, 1973) [in Russian].
11. J. M. Wallace and M. L. Blackmon, "Observations of low-frequency atmospheric variability," in *Large-Scale Dynamical Processes in the Atmosphere*, Ed. by B. J. Hoskins and R. P. Pearce (Academic Press, 1983), pp. 55–94.
12. A. V. Glazunov and V. P. Dymnikov, "Spatial spectra and characteristic horizontal scales of temperature and velocity fluctuations in the convective boundary layer of the atmosphere," *Izv., Atmos. Ocean. Phys.* **49** (1), 33–54 (2013).
<https://doi.org/10.1134/S0001433813010040>
13. A. Czaja and C. Frankignoul, "Observed impact of Atlantic SST anomalies on the North Atlantic Oscillation," *J. Clim.* **15** (6), 606–623 (2002).
[https://doi.org/10.1175/1520-0442\(2002\)015<0606:OIOASA>2.0.CO;2](https://doi.org/10.1175/1520-0442(2002)015<0606:OIOASA>2.0.CO;2)
14. R. Ding and J. Li, "Winter persistence barrier of sea surface temperature in the northern tropical Atlantic associated with ENSO," *J. Clim.* **24** (9), 2285–2299 (2011).
<https://doi.org/10.1175/2011JCLI3784.1>
15. C. Cassou, C. Deser, and M. A. Alexander, "Investigating the impact of reemerging sea surface temperature anomalies on the winter atmospheric circulation over the North Atlantic," *J. Clim.* **20** (14), 3510–3526 (2007).
<https://doi.org/10.1175/JCLI4202.1>
16. S. L. Taws, R. Marsh, N. C. Wells, et al., "Re-emerging ocean temperature anomalies in late-2010 associated with a repeat negative NAO," *Geophys. Res. Lett.* **38**, L20601 (2011).
<https://doi.org/10.1029/2011GL048978>
17. J. Buchan, J. J.-M. Hirschi, A. T. Blaker, et al., "North Atlantic SST anomalies and the cold North European weather events of winter 2009/10 and December 2010," *Mon. Weather Rev.* **142** (2), 922–932 (2014).
<https://doi.org/10.1175/MWR-D-13-00104.1>
18. M. Drévillon, L. Terray, P. Rogel, and C. Cassou, "Mid-latitude Atlantic SST influence on European winter climate variability in the NCEP reanalysis," *Clim. Dyn.* **18** (3–4), 331–344 (2001).
19. K. Hanawa and S. Sugimoto, "Reemergence areas of winter sea surface temperature anomalies in the world's oceans," *Geophys. Res. Lett.* **31** (10), L10303 (2004).
<https://doi.org/10.1029/2004GL019904>
20. M. A. Balmaseda, A. Vidard, and D. L. T. Anderson, "The ECMWF ocean analysis system: ORA-S3," *Mon. Weather Rev.* **136** (8), 3018–3034 (2008).
<https://doi.org/10.1175/2008MWR2433.1>
21. Y.-S. Chang, S. Zhang, A. Rosati, et al., "An assessment of oceanic variability for 1960–2010 from the GFDL ensemble coupled data assimilation," *Clim. Dyn.* **40** (3–4), 775–803 (2013).
<https://doi.org/10.1007/s00382-012-1412-2>
22. D. W. Behringer and Y. Xue, "Evaluation of the global ocean data assimilation system at NCEP: The Pacific Ocean," in *Proc. Eighth Symp. on Integrated Observing and Assimilation Systems for Atmosphere, Oceans, and Land Surface* (Seattle, 2004).
23. G. Garric, L. Parent, E. Greiner, et al., "Performance and quality assessment of the global ocean eddy-permitting physical reanalysis GLORYS2V4," in *EGU General Assembly Conference Abstracts* (2017), Vol. 19, p. 18776.
24. M. Ishii, M. Kimoto, and M. Kachi, "Historical ocean subsurface temperature analysis with error estimates," *Mon. Weather Rev.* **131** (1), 51–73 (2003).
[https://doi.org/10.1175/1520-0493\(2003\)131<0051:HOSTAW>2.0.CO;2](https://doi.org/10.1175/1520-0493(2003)131<0051:HOSTAW>2.0.CO;2)
25. S. A. Good, M. J. Martin, and N. A. Rayner, "EN4: Quality controlled ocean temperature and salinity profiles and monthly objective analyses with uncertainty estimates," *J. Geophys. Res.: Oceans* **118** (12), 6704–6716 (2013).
<https://doi.org/10.1002/2013JC009067>
26. V. Gouretski and F. Reseghetti, "On depth and temperature biases in bathythermograph data: development of a new correction scheme based on analysis of a global ocean database," *Deep-Sea Res. I* **57** (6), 812–833 (2010).
<https://doi.org/10.1016/j.dsr.2010.03.011>
27. G. Jenkins and D. Watts, *Spectral Analysis and Its Applications* (Holden Day, 1968; Mir, Moscow, 1971).
28. N. A. Diansky and P. A. Sukhonos, "Multidecadal variability of hydro-thermodynamic characteristics and heat fluxes in North Atlantic," in *Physical and Mathematical Modeling of Earth and Environment Processes* (Springer, Cham, 2018), pp. 125–137.
https://doi.org/10.1007/978-3-319-77788-7_14
29. The Lab Sea Group, "The Labrador Sea deep convection experiment," *Bull. Am. Meteorol. Soc.* **79** (10), 2033–2058 (1998).
30. P. A. Sukhonos and N. A. Diansky "Connections between the long-period variability modes of both temperature and depth of the upper mixed layer of the North Atlantic and the climate variability indices," *Izv.,*

- Atmos. Ocean. Phys. **56** (3), 300–311 (2020).
<https://doi.org/10.1134/S0001433820030111>
31. E. K. Schneider and M. Fan, “Observed decadal North Atlantic tripole SST variability. Part II: Diagnosis of mechanisms,” *J. Atmos. Sci.* **69** (1), 51–64 (2012).
 32. A. B. Polonsky and P. A. Sukhonos, “Influence of the North Atlantic Oscillation on the heat budget of the mixed layer in the North Atlantic,” *Russ. Meteorol. Hydrol.* **45** (9), 623–629 (2020).
 33. T. Ezer, G. L. Mellor, and R. J. Greatbatch, “On the interpentadal variability of the North Atlantic Ocean: Model simulated changes in transport, meridional heat flux and coastal sea level between 1955–59 and 1970–74,” *J. Geophys. Res.* **100** (C6), 10559–10566 (1995).
 34. H. L. Bryden, B. A. King, G. D. McCarthy, et al., “Impact of a 30% reduction in Atlantic meridional overturning during 2009–2010,” *Ocean Sci.* **10** (4), 683–691 (2014).
<https://doi.org/10.5194/os-10-683-2014>
 35. J. Marshall and G. Nurser, “On the recirculation of the subtropical gyre,” *Q. J. R. Meteorol. Soc.* **114** (484), 1517–1534 (1988).
 36. V. N. Stepanov, D. Iovino, S. Masina, et al., “Methods of calculation of the Atlantic meridional heat and volume transports from ocean models at 26.5° N,” *J. Geophys. Res.: Oceans* **121** (2), 1459–1475 (2016).
<https://doi.org/10.1002/2015JC011007>
 37. T. Ezer, “Detecting changes in the transport of the Gulf Stream and the Atlantic overturning circulation from coastal sea level data: The extreme decline in 2009–2010 and estimated variations for 1935–2012,” *Global Planet. Change* **129**, 23–36 (2015).
<https://doi.org/10.1016/j.gloplacha.2015.03.002>
 38. A. B. Polonsky and P. A. Sukhonos, “Mechanism for the formation of temperature anomalies in the upper layer of the North Atlantic,” *Oceanology (Engl. Transl.)* **58** (5), 652–660 (2018).
<https://doi.org/10.1134/S0001437018050120>
 39. V. Moron, R. Vautard, and M. Ghil, “Trends, interdecadal and interannual oscillations in global sea-surface temperatures,” *Clim. Dyn.* **14** (7), 545–569 (1998).
<https://doi.org/10.1007/s003820050241>
 40. R. T. Sutton and M. R. Allen, “Decadal predictability of North Atlantic sea surface temperature and climate,” *Nature* **388** (6642), 563–567 (1997).
 41. M. Årthun, T. Eldevik, E. Viste, et al., “Skillful prediction of northern climate provided by the ocean,” *Nat. Commun.* **8**, 15875 (2017).

Translated by N. Tret'yakova